

Restoring Narrow Linewidth to a Gradient-Broadened Magnetic Resonance by Inhomogeneous Dressing

Giuseppe Bevilacqua,¹ Valerio Biancalana,^{1,*} Yordanka Dancheva,² and Antonio Vigilante²

¹*Dept. of Information Engineering and Mathematics - DIISM, University of Siena - Italy*

²*Dept. of Physical Sciences, Earth and Environment - DSFTA, University of Siena - Italy*

(Dated: January 17, 2022)

We study the possibility of counteracting the line-broadening of atomic magnetic resonances due to inhomogeneities of the static magnetic field by means of spatially dependent magnetic dressing, driven by an alternating field that oscillates much faster than the Larmor precession frequency. We demonstrate that an intrinsic resonance linewidth of 25 Hz that has been broadened up to hundreds Hz by a magnetic field gradient, can be recovered by the application of an appropriate inhomogeneous dressing field. The findings of our experiments may have immediate and important implications, because they facilitate the use of atomic magnetometers as robust, high sensitivity detectors in ultra-low-field NMR imaging.

INTRODUCTION

We propose a method denominated *Inhomogeneous Dressing Enhancement of Atomic resonance* (IDEA) aimed at rendering optical atomic magnetometers suitable to work in an inhomogeneous magnetic field, such as those applied in ultra-low-field (ULF) NMR imaging. The method is based on dressing atoms by means of a strong magnetic field that oscillates transversely with respect to the (inhomogeneous) bias field around which they are precessing, at a frequency much larger than the local Larmor frequencies.

The magnetic dressing of precessing spins with a harmonic high frequency field was the subject of studies in the late Sixties, when a model based was developed on a quantum mechanical approach [1]. More recently, we re-examined this kind of system in the case of an arbitrary periodic dressing [2], making use of a perturbative approach based on the Magnus expansion [3] of the time-evolution operator. An interesting application of magnetic dressing was also studied very recently, in an experiment where critical dressing (matching the effective Larmor frequencies of different species) was applied to improve the sensitivity to small frequency shifts between two dressed species [4].

Magnetic resonance imaging (MRI) at ULF is an emerging method that uses high sensitivity detectors to measure the spatially encoded precession of pre-polarized nuclear spin ensembles in a microTesla- field [5].

Much like in conventional (high field) MRI, the spatial resolution can be achieved with parallelized measurements based on both frequency and phase encoding: a static inhomogeneity in the main field modulus causes the nuclear spin to precess at different frequencies dependent upon one co-ordinate (frequency encoding), while different initial conditions –imposed by pulsed gradients applied prior to the data acquisition– enable phase encoding, which is used to infer information for the two remaining co-ordinates.

The extremely low precession frequency makes the usual inductive pickup coils disadvantageous detectors in the ULF regime, while it enables the application of other kinds of detectors, such as superconducting quantum interference devices (SQUIDS) and optical atomic magnetometers (OAMs). These advanced sensors respond adequately to the low frequency signals characterizing the ULF regime, and may achieve sensitivities at $\text{fT}/\sqrt{\text{Hz}}$ level, rendering them state-of-the-art magnetometric sensors in MRI, as well as in other applications requiring extreme performance.

The feasibility of the ULF-MRI approach has been demonstrated with both this kinds of these non-inductive sensors [5, 6]. ULF MRI is compatible with the presence of other delicate instrumentation and the magnetic detectors can be used to record low-frequency magnetic signals originating from sources other than nuclear spins. In particular, hybrid instrumentation enabling multi-modal MRI and magnetoencephalography measurements has been proposed and implemented [7].

Compared to conventional MRI, ULF operation brings some relevant advantages. The ultimate spatial resolution of MRI is determined by the NMR linewidth, which in turn depends on the absolute field inhomogeneity. A modest relative homogeneity at ULF turns out to be excellent on the absolute scale: very narrow NMR lines with high signal-to-noise ratio can be recorded at ULF with apparatuses that are relatively simple from the point of view of field generation [8–10]. The encoding gradients for ULF MRI can also be generated by simple and inexpensive coil systems [11, 12]. Further important advantages of the ULF regime in MRI include the minimization of susceptibility artifacts [13] and the possibility of imaging in the presence of conductive materials [9, 14].

The sample-sensor coupling factor is a key feature, as in any NMR setup, and in the case of SQUID detectors the need for a cryostat may pose limitations. The latter issue makes the alternative choice of OAM detection attractive, together with the much lower maintenance costs

and the robustness of the OAM setup.

The OAM detection of NMR signals is based on probing the time evolution of optically pumped atoms that are magnetically coupled to the sample. In contrast to other solutions proposed, making use of flux transformers [15] and remote detection techniques [16], here we consider the case of atoms precessing in a static field that is superimposed upon a small term generated by nuclear spins precessing at a much lower rate. In this kind of in-situ MRI setup with OAM detection, the static field gradient applied to the sample for frequency encoding would also affect the atomic precession, with severe degradation of the OAM performance, unless a gradient discontinuity was introduced between the sample and sensor locations, with the need for coil geometries to hinder sample-sensor coupling.

We conceive, test and describe an approach allowing for the recording of narrow atomic resonances in spite of the presence of significant field inhomogeneity. IDEA is based on counteracting the atomic frequency spread caused by a defined field gradient by means of a spatially-dependent dressing of the atomic sample. Using this scheme in a MRI setup, the static and the (alternating) dressing fields inhomogeneously affect both the nuclear sample and the atomic sensor. However, marked selectivity occurs, because the effect of the dressing field depends on the gyromagnetic factor, so that the nuclear precession is substantially unaffected.

EXPERIMENTAL SETUP

The experimental setup (see Fig.1) is built around an OAM operating in a Bell & Bloom configuration, described in detail in Ref.[17].

Briefly, the OAM uses Cs vapor optically pumped into a stretched (maximally oriented) state by means of laser radiation at the milli-Watt level. This pump radiation is circularly polarized and tuned to the Cs D_1 line. The time evolution of the atomic state is probed by a co-propagating weak (micro-Watt level) and linearly polarized beam, tuned to the proximity of the D_2 line. A transverse magnetic field B_0 causes a precession of the induced magnetization. The magnetization decay is counteracted via synchronous optical pumping, which is obtained by modulating the pump laser wavelength at a frequency $\omega_M/2\pi$, which is resonant with the Larmor frequency $\Omega_L/2\pi$. Scanning ω_M around Ω_L makes it possible to characterize the resonance profile. In operative conditions, a resonance width of about $\Gamma = 25$ Hz HWHM is measured.

The precession causes a time-dependent Faraday rotation of the probe radiation. This Faraday rotation is driven to oscillate at ω_M (forcing term), to which it responds with a phase $\varphi(t)$ depending on the detuning $\delta = \omega_M - \Omega_L = \omega_M - \gamma B$ (γ is the gyromagnetic factor)

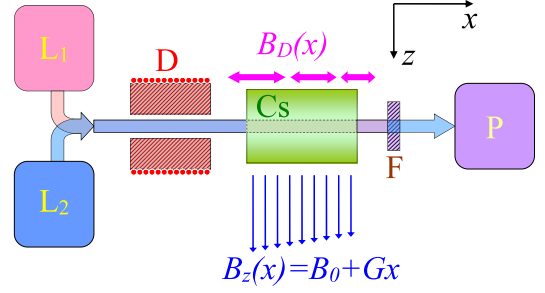


Figure 1. Simplified schematics of the magnetometer and of the field arrangement (L_1 - pump laser; L_2 probe laser; Cs - Cesium cell; F - interference filter stopping the pump radiation; P - balanced polarimeter). The optical axis of the sensor is x . A static magnetic field - oriented in z direction - with the main component dependent on the x co-ordinate due to a static quadrupolar term, producing a gradient $G = \partial B_z / \partial x$. The concomitant $\partial B_x / \partial z$ term has no first order effects on the atomic precession. An electromagnetic dipole D oriented along x produces an oscillating (dressing) magnetic field B_D at a frequency well above the Larmor frequency, oriented along x , the strength of which decays along that direction.

so as to evolve in accordance with the magnetic field B . Following interaction with the vapour, the pump radiation is stopped by an interference filter, and the magnetic field and its variation are extracted from the Faraday rotation of the probe beam, as measured by a balanced polarimeter. The sensor, without any passive shielding, operates in a homogeneous B_0 field, which is obtained by partially compensating the environmental field and is oriented along the z axis. B_0 has a typical strength of $4 \mu\text{T}$, giving $T_L = 2\pi/\Omega_L \approx 71 \mu\text{s}$.

The atomic vapor (Cs) is contained in a sealed cell with 23 Torr N_2 as a buffer gas, determining a diffusion coefficient $D=3.23 \text{ cm}^2/\text{s}$ [18], which in a precession period causes transverse displacements $\delta = (2DT_L/3)^{1/2} \approx 0.12 \text{ mm}$. The laser beam is $\Phi \approx 1 \text{ cm}$ in diameter, and the condition $\Phi \gg \delta$ enables gradiometric measurements with a base-line of about 5 mm by analyzing the probe spot in two halves [17].

Any increase in the resonance width has detrimental effects on magnetometric sensitivity, rendering it of primary importance to counteract any broadening mechanism. The equation of motion of the magnetization is

$$d\vec{M} = - \left(\gamma \vec{B} \times \vec{M} + D \nabla^2 \vec{M} + \Gamma \vec{M} \right) dt. \quad (1)$$

In the case of an inhomogeneous field, the first term in parenthesis is position-dependent and leads to line broadening unless the second (diffusion) term is large enough to make all the atoms behave as if they were precessing around an average field. Indeed, operating with low-pressure cells (i.e. a large D coefficient) may help to counteract gradient-induced resonance broadening, thanks to the so-called motional narrowing (MN)

phenomenon [19, 20]. The MN requires anti-relaxation coating to prevent an increase of the third term in parenthesis due to atom-wall collisions. In the MN regime, the linewidth quadratically depends on the field inhomogeneity, so that MN is only effective with adequately weak gradients. As an example (see Eq.62 in ref [19]) using a vacuum cell 2cm in size, MN would maintain a width below Γ only for $G < 2\text{nT/cm}$. We consider the opposite case, in which the presence of buffer gas makes the diffusion coefficient quite small. With this limit, besides achieving a local response (with the sub-millimetric δ mentioned above), non-broadened local resonances are obtained, provided that the frequency variation caused by diffusion displacement in a precession period T_L is negligible with respect to the intrinsic width Γ , i.e. under the condition $G \ll (\sqrt{3}\Gamma)/(\gamma\delta) \approx 1\text{ }\mu\text{T/cm}$, which is much less stringent than that for the MN.

METHOD

The main goal of this work is to counteract the sensitivity degradation of an OAM using a buffered sensor cell in the high-pressure regime, which is placed in a strong linear (quadrupole) magnetic field gradient such as that used for MRI frequency encoding [21].

The method is based on magnetically dressing atoms whose angular momentum is precessing in a static field. This dressing consists in applying a strong time-dependent field that is oriented perpendicularly to the static field and oscillates at a frequency well above the Larmor frequency. Under these conditions, the two momentum components perpendicular to the dressing field evolve in a rather complicated manner, under its direct and time-dependent effect, while the component along the dressing field is not directly coupled and keeps oscillating harmonically, but at an effective Larmor frequency $\Omega_D < \Omega_L$. To this end, a transverse oscillating field B_D , with inhomogeneity along the x direction, is applied by means of a dipole D oriented along x (as represented in Fig.1). Its concomitant gradients produce both transverse (y) and longitudinal (z) oscillating components in the off-axis interaction region. However, these spurious terms have negligible effects.

Fig.1 represents the arrangement for dc (bias, B_z) and ac (dressing, B_D) field application. The coils for static field and field gradient control are not represented, and the schematics of the optical part are also simplified. B_z is oriented along z and its gradient $G = \partial B_z / \partial x$ is set by permanent magnets arranged in a quadrupolar configuration. Thus, the Larmor frequency set by B_z is position-dependent along the optical axis x .

The dipolar field B_D is produced by a solenoid wound around a ferrite nucleus to generate B_D oriented along x , with an amplitude decreasing in that direction. The ferrite nucleus has a hollow-cylinder shape, which permits

precise alignment without hindering the propagation of the laser beams.

The dressing field B_D oscillates harmonically and has an axial component

$$B_D(x, t) = \frac{\mu_0}{2\pi} \frac{m(t)}{(x_0 + x)^3} = B_{D0}(x) \cos(\omega t), \quad (2)$$

where μ_0 is the vacuum permittivity, $m(t) = m_0 \cos(\omega t)$ is the oscillating dipole momentum, x_0 is the position of the sensor with respect to the dipole along its axis and x is the displacement from the sensor center. A time-dependent current oscillating at $\omega \gg \gamma B_z(x) = \Omega_L(x)$ induces a magnetic dipole with adjustable intensity. The ferrite and the use of a resonant circuit help to produce a strong oscillating field (several μT , in our case).

The field B_D alters the time evolution of the atomic magnetization in such way as to make its x component oscillate harmonically at a dressed (reduced) angular frequency with respect to its unperturbed precession around the static field [2]:

$$\Omega_D(x) = \Omega(x) J_0(\gamma B_{D0}(x)/\omega), \quad (3)$$

where $J_i(z)$ is the i -th Bessel function of the first kind.

The spatially-dependent dressing can compensate the B_z inhomogeneity in a first order approximation. In fact, being $B_z \approx B_0 + Gx$,

$$\begin{aligned} \Omega_D(x) &= \Omega_D(0) + \Omega'_D(0)x + \frac{1}{2}\Omega''_D(0)x^2 + O(x^3) = \\ &= \gamma B_0 J_0(\alpha) + \gamma [3B_0\alpha J_1(\alpha) + Gx_0 J_0(\alpha)] \frac{x}{x_0} \\ &\quad - \frac{3\alpha\gamma}{2} [(B_0 - 2Gx_0)J_1(\alpha) + 3\alpha B_0 J_0(\alpha)] \left(\frac{x}{x_0}\right)^2 \\ &\quad + O((x/x_0)^3) \end{aligned}$$

where $\alpha = (\mu_0/2\pi)(\gamma m_0)/(\omega x_0^3)$, and the condition for compensating the gradient G is thus

$$G = -3 \frac{B_0}{x_0} \frac{\alpha J_1(\alpha)}{J_0(\alpha)}, \quad (4)$$

which, for values α of experimental interest (up to $\alpha \approx 1$), results in G values up to $1.7(B_0/x_0)$.

Under compensated conditions (Eq.4), in the second order approximation the angular frequency has the expression

$$\Omega_D(x) \simeq \gamma B_0 \left[J_0 - \beta \left(\frac{x}{x_0}\right)^2 \right] \quad (5)$$

with $\beta = (3\alpha/2J_0)(J_0J_1 + 6\alpha J_1^2 + 3\alpha J_0^2)$, and $J_i = J_i(\alpha)$.

It is worth noting that β is non-null for any α , meaning that a *Helmholtz condition* (zeroed quadratic term) would require the application of a secondary –weaker– oscillating dipole placed at an opportune, smaller distance on the opposite side of the cell.

RESULTS

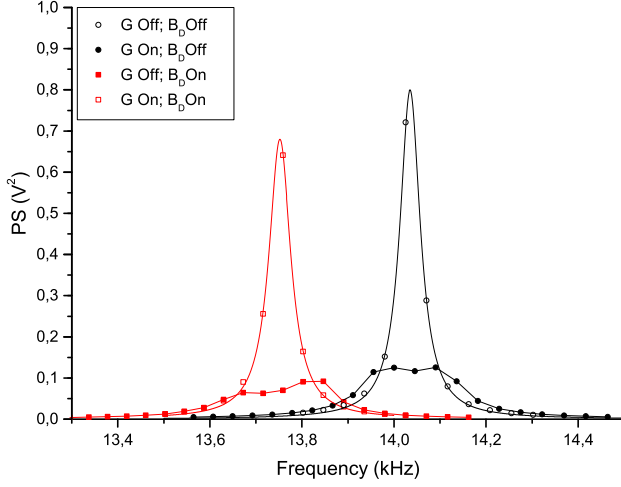


Figure 2. Atomic magnetic resonance under different conditions. The plot (○) shows the unperturbed resonance; (●) in the presence of a static magnetic field gradient; (■) is obtained with no static gradient, but in the presence of a strong, transverse, inhomogeneous field which oscillates much faster than the Larmor precession ($\omega = 2\pi 32$ kHz). This dressing field (amplitude of about $2.4 \mu\text{T}$) produces a resonance shift that broadens the resonance due to its inhomogeneity (600 nT/cm). With opportune amplitude and frequency values of the dressing field, the two broadening mechanisms compensate each other, and a shifted but narrow resonance can be recorded, as shown in the plot (◻).

We present in Fig.2 a set of spectra obtained under four different conditions, namely in the presence of: a static gradient; the same gradient and appropriate dressing compensation; the same dressing, having removed the static gradient; and with the static homogeneous field alone. The plot (○) in Fig.2 shows the power spectrum (PS) of the unperturbed resonance in the absence of the gradient and dressing field and under optimal operating conditions. At $B_0 = 4 \mu\text{T}$ the magnetic resonance amplitude shows a peak at about 14 kHz with a half-width-half-maximum of $\Gamma \approx 25$ Hz. When a quadrupolar magnetic gradient $G = \partial B_z / \partial x = 40$ nT/cm is introduced, the resonance gets broader as shown in the plot (●) in Fig.2.

In the same figure, the plot (■) is obtained in the presence of a strong transverse inhomogeneous field that oscillates much faster than the Larmor precession ($\omega = 2\pi 32$ kHz) and in the absence of the static gradient. The dressing field B_D has an amplitude of about $2.4 \mu\text{T}$: it shifts the resonance, and –due to the inhomogeneity– broadens it, as well. Under appropriate conditions (Eq.4), the two broadening mechanisms compensate each other to the first order, and a shifted but narrow resonance can be recorded, as shown in plot (◻). The solid

lines are Lorentzian best fits in the cases of narrow resonances (no gradient and dressing-compensated gradient) and eye-guiding interpolations for the two broadened profiles, respectively.

When increasing the values of G , the second order term in Eq.5 becomes progressively more important, and the dressing optimization cannot fully restore the original linewidths. Fig.3 shows the resonance profiles (under the condition Eq.4) for different values of G . For the larger values of G (and consequently stronger dressing), the non-linear term of Eq.5 causes a deformation of the resonance profile, with the left wing slightly exceeding the Lorentzian values. Even with very large G

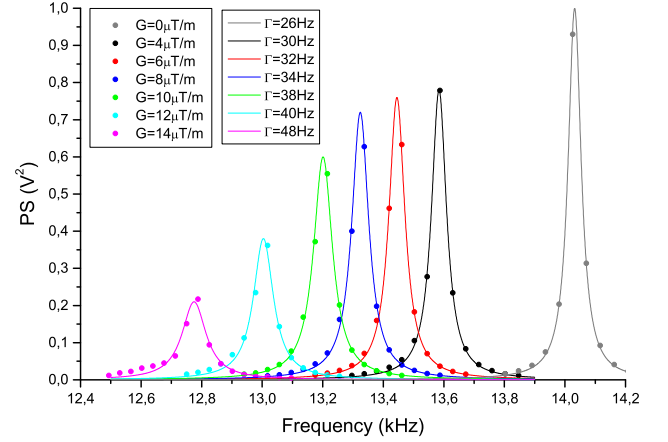


Figure 3. Resonance profile under suppressed-broadening conditions, for different values of G . The dots are the amplitudes measured and the lines are best fits targeted to a Lorentzian profile. A progressive shift towards lower frequencies occurs, consistently with Eq.3. Simultaneously, the profile width increases slightly. Above 100 nT/cm, some deviations from the Lorentzian model, due to the higher order terms (Eq.5), appear as an increase in the low-frequency wing. The leftmost plot (recorded at 140 nT/cm) would appear as a 1 kHz broadened resonance in the absence of the dressing field.

values, the line broadening is effectively compensated: with $G = 80$ nT/cm a 34 Hz linewidth (8 Hz broadening) is achieved, compared with the 560 Hz that would be observed without the dressing field.

APPLICATION TO MRI

We tested the IDEA in a preliminary MRI experiment using remotely polarized protons in tap water, adopting the setup described in Refs.[22, 23]. Water protons contained in a 4 ml cartridge (pictured in the upper part of Fig.6) were prepolarized in a 1 T field and shuttled to the proximity of the sensor [24]. The experiment was carried out in unshielded environment, where the environmental magnetic noise was preliminarily re-

duced using an active stabilization [25] method and then cancelled by measuring differentially on a 5 mm baseline. An automated system permits long-lasting repeated measurements [22], requiring synchronous control of the shuttling system and video-camera checks of its performance; the activation and deactivation of the driving field and field-stabilization system; the application of tipping ($\pi/2$) pulses; DAQ and data elaboration.

The dressing factor (Eq.3) is negligible for the precessing protons due to their much lower gyromagnetic factor, so that in the presence of a static gradient their magnetization precesses at a frequency that depends only on the local static field, as in any frequency-encoded MRI experiment. The time-domain signal recorded appears as shown in Fig.4, with and without the static gradient, respectively.

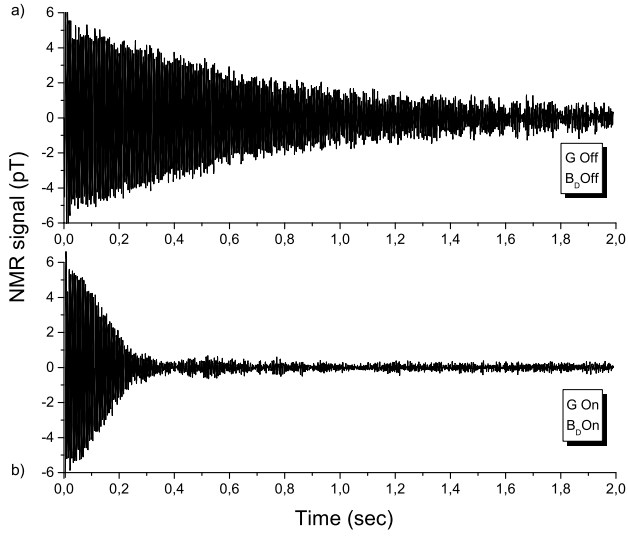


Figure 4. NMR signal from 4ml H₂O sample. Plot a) shows the NMR signal in a homogeneous field with neither G nor B_D applied. The trace was obtained by averaging over 100 shots. Plot b) shows the NMR signal recorded in the presence of $G = 50$ nT/cm and $B_D = 3$ μ T. The trace is obtained by averaging over 400 shots.

Fig.5 shows the effect of the static and dressing field inhomogeneities on the spectra of the proton NMR signal. Plot (a) is obtained in a homogeneous static field while applying a dressing field. The nuclear signal is insensitive to B_D while the dressed Cs atoms have position-dependent resonance, so that only a small fraction (slice) are synchronously pumped and effectively contribute to detect the NMR signal. The resonance recorded has the same width but a worse S/N compared to that resulting for $G = 0$ and $B_D = 0$ (plot b). The application of a static field G broadens both the atomic and the NMR resonances. However, (plot c) the whole atomic sensor contributes to a broadened NMR signal detection with a good S/N, thanks to IDEA method restoring the atomic resonance linewidth while enabling the registra-

tion of position-dependent NMR.

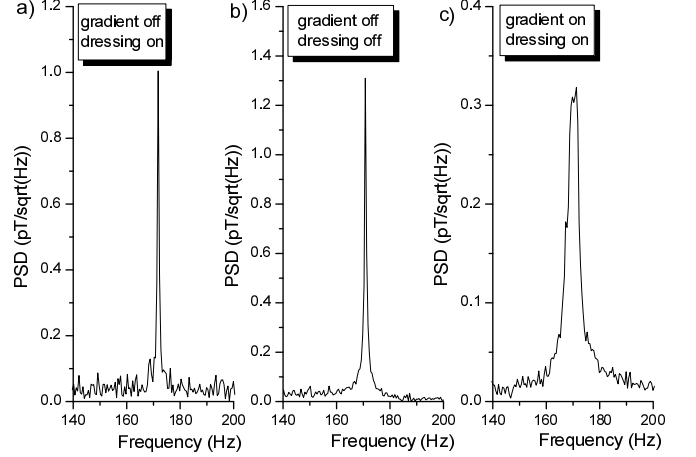


Figure 5. Tap-water proton NMR spectra of the signals under different gradient conditions. Plot a) is obtained with $G = 0$ and $B_D = 3$ μ T: a narrow NMR is recorded, with low S/N, because the protons are not affected by B_D , while Cs atoms are, so that only a slice of the sensor is effectively pumped. Plot b) is obtained from the data shown in Fig.4 a): $G = 0$ and $B_D = 0$ produce narrow NMR with good S/N. Plot c) corresponds to the trace shown in Fig.4 b): here the static gradient G broadens the NMR spectrum. The IDEA method allows the same same spectrum to be recorded with a good S/N.

The NMR signal recorded in the presence of the gradient G can be modeled as:

$$S(t) = e^{(-\Gamma_N - i\omega_0)t} \int_{-\infty}^{\infty} \eta(x) \rho(x) e^{i\gamma_N G x t} dx, \quad (6)$$

where $\eta(x)$ represents the detection efficiency determined by the sample-sensor coupling and $\rho(x)$ is the proton density in the sample. Following a standard signal elaboration, after scaling the data by $\exp(\Gamma_N t)$, a Fourier transform is used to reproduce the shape of $\eta(x)\rho(x)$. This is the analysis conducted on the data corresponding to the plots (b) in Figs.4 and 5 in order to reconstruct the $\eta\rho$ profile shown in Fig.6. An estimate of $\eta(x)$ is made, on the basis of the geometry of our experimental setup, and used to infer the 1-D image $\rho(x)$ shown in the same figure.

CONCLUSION

We have proposed, characterized and tested a method (IDEA), based on magnetically dressing atomic ground-states, which enables an atomic magnetometer to operate in the presence of a strong field gradient while preserving its sensitivity, thanks to the suppression of gradient-induced resonance broadening.

We found accordance between the theoretical model and the resonance behavior observed.

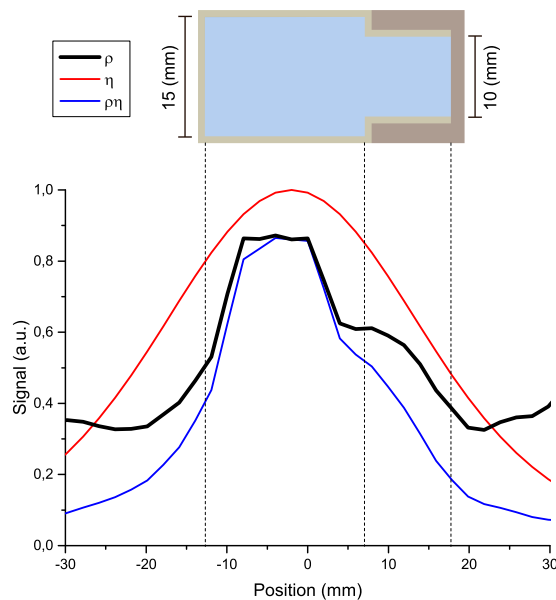


Figure 6. Plots of the measured $\rho(x)\eta(x)$ (blue), the estimated $\eta(x)$ (red) and the inferred $\rho(x)$ (black), which can be compared with the sample shape represented in the upper part. The data are the same as shown in the plots b) of Figs.4 and 5. Some position jitter of the sample occurs and is detected shot-by-shot by the camera. To limit the consequent image blurring, only traces corresponding to sample positioning within a ± 3 mm interval were selected.

We have provided a preliminary demonstration of the applicability of the IDEA method in recording unidimensional NMR images of remotely polarized protons in the ULF regime.

Our findings suggest that the IDEA method constitutes a promising tool in ULF MRI using atomic magnetometers. The IDEA method could also be applied in shielded volumes, and in conjunction with phase-encoding techniques, making several kinds of optical magnetometers suitable for use in 3-D MRI apparatuses, in spite of the large gradients that must be applied to achieve fine spatial resolution.

ACKNOWLEDGEMENTS

The authors are pleased to thank Alessandra Retico for the useful and interesting discussions and Emma Thorley for improving the text.

* valerio.biancalana@unisi.it

[1] S. Haroche, C. Cohen-Tannoudji, C. Audoin, and J. P. Schermann, “Modified Zeeman hyperfine spectra observed in ^1H and ^{87}Rb ground states interacting with a

nonresonant RF field,” *Phys. Rev. Lett.*, vol. 24, pp. 861–864, 1970.

- [2] G. Bevilacqua, V. Biancalana, Y. Dancheva, and L. Moi, “Larmor frequency dressing by a nonharmonic transverse magnetic field,” *Phys. Rev. A*, vol. 85, p. 042510, Apr. 2012.
- [3] W. Magnus, “On the exponential solution of differential equations for a linear operator,” *Communications on Pure and Applied Mathematics*, vol. 7, no. 4, pp. 649–673, 1954.
- [4] C. M. Swank, E. K. Webb, X. Liu, and B. W. Filippone, “Spin Dressed Relaxation and Frequency Shifts from Field Imperfections,” *ArXiv e-prints*, Aug. 2018.
- [5] V. S. Zotev, A. N. Matlashov, P. L. Volegov, A. V. Urbaitis, M. A. Espy, and R. H. K. Jr, “SQUID-based instrumentation for ultralow-field MRI,” *Superconductor Science and Technology*, vol. 20, no. 11, p. S367, 2007.
- [6] I. Savukov and T. Karaulanov, “Anatomical MRI with an atomic magnetometer,” *Journal of Magnetic Resonance*, vol. 231, pp. 39 – 45, 2013.
- [7] P. T. Vesonen, J. O. Nieminen, K. C. J. Zevenhoven, J. Dabek, L. T. Parkkonen, A. V. Zhdanov, J. Luomahaara, J. Hassel, J. Penttilä, J. Simola, A. I. Ahonen, J. P. Mäkelä, and R. J. Ilmoniemi, “Hybrid ultra-low-field MRI and magnetoencephalography system based on a commercial whole-head neuromagnetometer,” *Magnetic Resonance in Medicine*, vol. 69, no. 6, pp. 1795–1804, 2012.
- [8] R. McDermott, A. H. Trabesinger, M. Mück, E. L. Hahn, A. Pines, and J. Clarke, “Liquid-state NMR and scalar couplings in micro-Tesla magnetic fields,” *Science*, vol. 295, no. 5563, pp. 2247–2249, 2002.
- [9] A. N. Matlachov, P. L. Volegov, M. A. Espy, J. S. George, and R. H. Kraus, “SQUID detected NMR in micro-Tesla magnetic fields,” *Journal of Magnetic Resonance*, vol. 170, no. 1, pp. 1 – 7, 2004.
- [10] M. Burghoff, S. Hartwig, L. Trahms, and J. Bernarding, “Nuclear magnetic resonance in the nano-Tesla range,” *Applied Physics Letters*, vol. 87, no. 5, p. 054103, 2005.
- [11] R. McDermott, S. Lee, B. t. Haken, A. H. Trabesinger, A. Pines, and J. Clarke, “Micro-Tesla MRI with a superconducting quantum interference device,” *Proceedings of the National Academy of Sciences*, vol. 101, no. 21, pp. 7857–7861, 2004.
- [12] V. S. Zotev, A. N. Matlachov, P. L. Volegov, H. J. Sandin, M. A. Espy, J. C. Mosher, A. V. Urbaitis, S. G. Newman, and R. H. Kraus, Jr, “Multi-channel SQUID system for MEG and ultra-low-field MRI,” *IEEE Trans. Appl. Supercond.*, vol. 17, pp. 839–842, 2007.
- [13] S. K. Lee, M. Mölle, W. Myers, N. Kelso, A. H. Trabesinger, A. Pines, and J. Clarke, “SQUID-detected MRI at 132 μT with T1-weighted contrast established at 10 μT -300 mT,” *Magnetic Resonance in Medicine*, vol. 53, no. 1, pp. 9–14, 2004.
- [14] M. Mölle, S.-I. Han, W. R. Myers, S.-K. Lee, N. Kelso, M. Hatridge, A. Pines, and J. Clarke, “SQUID-detected micro-Tesla MRI in the presence of metal,” *Journal of Magnetic Resonance*, vol. 179, no. 1, pp. 146 – 151, 2006.
- [15] I. Savukov and T. Karaulanov, “Magnetic-resonance imaging of the human brain with an atomic magnetometer,” *Applied Physics Letters*, vol. 103, no. 4, p. 043703, 2013.
- [16] S. Xu, V. V. Yashchuk, M. H. Donaldson, S. M. Rochester, D. Budker, and A. Pines, “Magnetic res-

- onance imaging with an optical atomic magnetometer,” *Proceedings of the National Academy of Sciences*, vol. 103, no. 34, pp. 12668–12671, 2006.
- [17] G. Bevilacqua, V. Biancalana, P. Chessa, and Y. Dancheva, “Multichannel optical atomic magnetometer operating in unshielded environment,” *Applied Physics B*, vol. 122, no. 4, p. 103, 2016.
- [18] F. A. Franz and C. E. Sooriamoorthi, “Spin relaxation within the $6^2P_{\frac{1}{2}}$ and $6^2S_{\frac{1}{2}}$ states of cesium measured by white-light optical pumping,” *Phys. Rev. A*, vol. 10, pp. 126–140, Jul 1974.
- [19] G. D. Cates, S. R. Schaefer, and W. Happer, “Relaxation of spins due to field inhomogeneities in gaseous samples at low magnetic fields and low pressures,” *Phys. Rev. A*, vol. 37, pp. 2877–2885, Apr 1988.
- [20] S. Pustelny, D. F. Jackson Kimball, S. M. Rochester, V. V. Yashchuk, and D. Budker, “Influence of magnetic-field inhomogeneity on nonlinear magneto-optical resonances,” *Phys. Rev. A*, vol. 74, p. 063406, Dec 2006.
- [21] R. Ansorge and M. Graves, *The Physics and Mathematics of MRI*. 2053-2571, Morgan and Claypool Publishers, 2016.
- [22] G. Bevilacqua, V. Biancalana, Y. Dancheva, A. Vigilante, A. Donati, and C. Rossi, “Simultaneous detection of H and D NMR signals in a micro-Tesla field,” *The Journal of Physical Chemistry Letters*, vol. 8, pp. 6176–6179, 2017. PMID: 29211488.
- [23] G. Bevilacqua, V. Biancalana, A. Ben Amar Baranga, Y. Dancheva, and C. Rossi, “Micro-Tesla NMR J-coupling spectroscopy with an unshielded atomic magnetometer,” *Journal of Magnetic Resonance*, vol. 263, pp. 65–70, 2016.
- [24] Biancalana, Valerio, Dancheva, Yordanka, and Stiaccini, Leonardo, “Note: A fast pneumatic sample-shuttle with attenuated shocks,” *Review of Scientific Instruments*, vol. 85, no. 3, pp. –, 2014.
- [25] G. Bevilacqua, V. Biancalana, Y. Dancheva, and A. Vigilante, “Self-adaptive loop for external disturbance reduction in differential measurement set-up,” *ArXiv*, vol. 1803.03212, 2018.